Basic Science
Research Paper

OPEN

PAIN REPORTS

Functional magnetic resonance imaging insights into nociceptive signal processing network in rat lumbar spinal cord

Xuerong Zhang[a,b], Chaoqi Mu[a,b], Arabinda Mishra[a,c], Feng Wang[a,c], Pai-Feng Yang[a,c], Xinqiang Yan[a,c], Ming Lu[a,c], John C. Gore[a,b,c], Li Min Chen[a,b,c,*]

Abstract

Introduction and Objectives: High-resolution functional magnetic resonance imaging (fMRI) allows the mapping of functional organization of intraspinal circuits. This study aimed to identify nociceptive heat processing regions within the gray matter of the lumbar spinal cords and delineate their functional organization using task and resting-state fMRI in rats under anesthesia.

Methods: High-resolution fMRI BOLD data were acquired from L3-L5 spinal segments during noxious heat (47.5°C) stimulation of the left hind paw and at rest at 9.4T MRI.

Results: Noxious heat-elicited BOLD signal increases were detected at deep layers of dorsal horns and intermediate zone within the rostral lumbar enlargement (L3) and deep layers of the ipsilateral dorsal horn in lumbar segment L4. Resting-state functional connectivity (rsFC) analysis revealed the strongest rsFC strengths between dorsal–dorsal and ventral–ventral horns within each lumbar segment. No significant rsFC was found between the horns in different segments.

Conclusion: Our results demonstrate that lumbar enlargement (L3 and L4) was involved in processing heat nociceptive information and bilateral dorsal and ventral horns were strongly interconnected at rest. We hypothesize that the intermediate zone in the rostral subsegment of L3 serves as a modulation center for nociceptive processing within the lumbar cord.

Keywords: fMRI, Rat, Lumbar spinal cord, Noxious heat, Resting-state functional connectivity

1. Introduction

Functional magnetic resonance imaging (fMRI) studies of the spinal cord are technically challenging but provide novel insights into spinal cord functions, its functional architecture, as well as circuits for information processing, integration, and modulation within the spinal cord. We have previously published several reports demonstrating the use of multiparametric MRI to characterize the functional and structural features of the cervical spinal cord in rodents, nonhuman primates, and humans.[7,35,48,49,51] Their findings not only demonstrated the power of fMRI for studying spinal cord functional architecture but also revealed that there are differences in the functional organization pattern across species. Previous spinal cord fMRI studies have revealed nociception-related activity in the dorsal horn and demonstrated functional connectivity with supraspinal regions,[12,20,21,37,38] providing insights into central pain modulation. Most of this work has focused on the cervical spinal cord.

The ability of fMRI to noninvasively image the lumbar spinal cord is significant because lumbar cord mediates sensory and motor behavior of the lower body, including the hindlimbs.[3] Pain signals from peripheral nociceptive fibers are first modulated in the spinal cord dorsal horn by interneurons before ascending to the brain.[50] The mechanisms of normal pain processing in the lumbar spinal cord are complex.[10,22] Given the high prevalence of pain associated with the pathologies of the lumbar spinal cord, such as lower back pain and neuropathic pain related to spinal cord injury, an improved understanding of the mechanisms of pain processing within the lumbar spinal cord could provide novel

Sponsorships or competing interests that may be relevant to content are disclosed at the end of this article.

[a] Vanderbilt University Institute of Imaging Science, Nashville, TN, USA, [b] Department of Biomedical Engineering, Vanderbilt University, Nashville, TN, USA, [c] Department of Radiology and Radiological Sciences, Vanderbilt University Medical Center, Nashville, TN, USA

**Corresponding author. Address: Department of Radiology and Radiological Sciences, Vanderbilt University Medical Center, Nashville, TN 37232. Tel.: (615) 936-7069. E-mail address: limin.chen@vanderbilt.edu (L. M. Chen).*

Copyright © 2026 The Author(s). Published by Wolters Kluwer Health, Inc. on behalf of The International Association for the Study of Pain. This is an open access article distributed under the terms of the Creative Commons Attribution-NonCommercial-ShareAlike License 4.0 (CC BY-NC-SA) which allows others to remix, tweak, and build upon the work non-commercially, as long as the author is credited and the new creations are licensed under the identical terms.

PR9 11 (2026) e1368

http://dx.doi.org/10.1097/PR9.0000000000001368

insights for developing effective pain management strategies including spinal cord stimulation and could also provide a basis for understanding changes that occur after injury and in diseases.

Preclinical studies using animal disease models provide novel mechanistic insights about pain processing that are often difficult to obtain directly from patients.[14] These insights can include information that guides treatments such as spinal cord stimulation.[30] In this study, we aimed to identify the nociceptive processing regions using fMRI and delineate their functional connections using resting-state functional connectivity (rsFC) measures within lumbar spinal cords of rats. Here, we report our findings of the network of responses to heat-induced pain within the lumbar region and intraspinal circuits among gray matter (GM) horns.

2. Methods

2.1. Materials and animal preparation

Nine adult male Sprague-Dawley rats (7–10 week old, 300 ± 20 g) were used in this study. During each scan, each rat was initially sedated by inhaling 3% isoflurane carried by oxygen through a nose cone. The rats were secured in a customized cradle in a supine position, with the lumbar spine positioned at the center of a custom quadrature surface coil. The rectal temperature and respiratory cycles of rats were continuously monitored and maintained within a normal physiological range. The isoflurane anesthesia level was maintained at 1% to 1.3%, delivered through O_2 during fMRI scans. All procedures were performed following the NIH guideline and protocol approved by the Institutional Animal Care and Use Committee of Vanderbilt University.

2.2. In vivo MRI data acquisition

All MR images were acquired using a 9.4T Bruker scanner with a custom quadrature transmit-receive surface coil of 2 centimeters in diameter.[27] After shimming, 5 contiguous axial slices (in 3 mm thickness) of anatomical magnetization transfer contrast (MTC) images were collected before fMRI data acquisition, with the third slice positioned approximately over the lumbar enlargement (**Fig. 1A**). To assist in localizing the lumbar enlargement, we also obtained MTC images in sagittal and coronal planes using a gradient echo acquisition (repetition time (TR)/echo time (TE) = 200/3 ms; number of excitations = 4 [axial], 8 [sagittal],12 [coronal]; matrix size = 128 × 128; field of view = 32 × 32 mm^2; slice thickness at 0.75 mm [sagittal] or 0.5 mm [coronal]; and flip angle = 35°) (**Fig. 1B**). Based on rat spinal cord neuroanatomy[42] and MRI acquisition slice thickness, we estimated that the 5 axial slices cover the L3-L5 spinal cord segments.

Functional magnetic resonance imaging scans were acquired in both resting-state and heat stimulation conditions, using a multi-shot gradient echo planar imaging sequence (TR/TE = 3000/~6.70 ms, 6-shot acquisition with 500 ms per shot, matrix size = 128 × 128, field of view = 32 × 32 mm^2, in-plane resolution at 0.25 × 0.25 mm^2). Each resting-state run contained 180 volumes while each heat stimulation run contained 145 volumes and 9 epochs of 15 seconds of 47.5°C noxious heat-on and 30 seconds of stimulus-off periods (**Fig. 1C**). A 47.5°C noxious heat stimulus was delivered to the rat's left hind paw with an MRI-compatible thermal probe (3 cm in diameter, Medoc Advanced Medical Systems, Ramat Yishai, Irasel). Heat stimulus started from a baseline temperature of 32°C and reached the target temperature within 1 second with a heating rate of 70°C/second. A typical imaging session involved 3 resting-state runs, 3 heat stimulus runs, followed by 2 additional resting-state runs (**Fig. 1C**).

2.3. Functional magnetic resonance imaging image processing and statistical analyses

2.3.1. Data preprocessing

All the fMRI data were initially preprocessed using MATLAB and followed by 3D motion correction, slice-by-slice motion

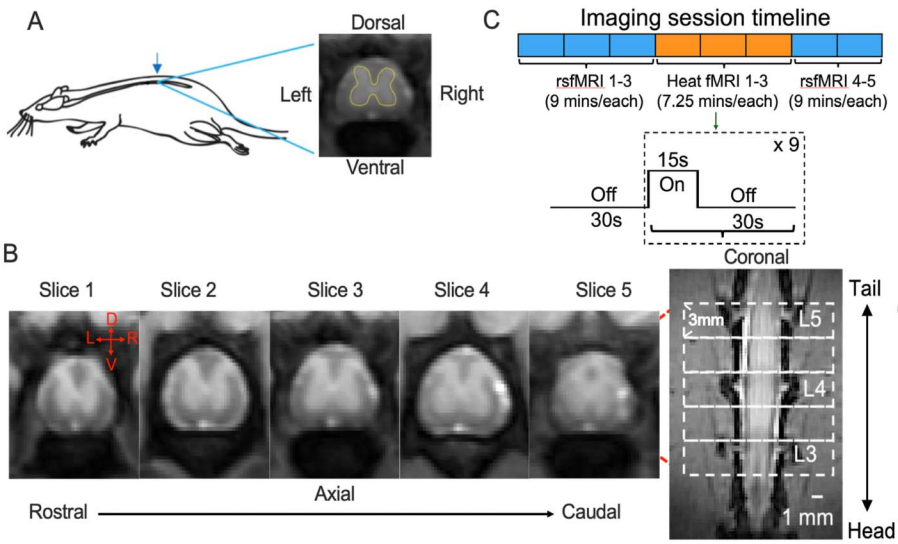

Figure 1. High-resolution magnetization transfer contrast (MTC)-weighted anatomical images of the L3–L5 spinal cord from a representative rat. (A) Left: schematic illustration of the research interest of lumbar spinal cord. Right: A typical axial slice of MTC image of lumbar spinal cord with the gray–white matter boundary outlined by yellow lines. (B) Left: 5 axial MTC images acquired with slice 3 centered at the L3/L4 segment. Right: the corresponding axial slice positions overlaid on the coronal image in the middle line. (C) Schematics of 1 imaging session timeline and noxious heat stimulus presentation paradigm. D, dorsal; L, left; R, right; V, ventral.

correction, and slice time correction in FMRIB Software Library.[36] A low-pass filter with a cutoff frequency of 0.13 Hz was applied to the resting-state fMRI (rsfMRI) BOLD signal time series. Nuisance signals such as motion parameters and muscle signals were regressed out. The RETROICOR method was used to remove respiratory noise. Muscle masks were manually drawn. We applied quality control and excluded runs with motion parameters exceeding 1 mm and resting-state fMRI runs with temporal signal-to-noise ratio (tSNR) below 5 from analysis. For group-level analysis, the echo planar imaging from each animal were first aligned to MTC images acquired within the same session and then registered to a template for quantification in FMRIB Software Library. This template was the anatomical MTC image of a representative rat, which presents a clear depiction of spinal cord structure.

2.3.2. Heat stimulus-driven functional magnetic resonance imaging data analysis

For heat stimulus-driven fMRI data, all runs were analyzed at both individual and group levels using SPM12. Individual-level analyses were performed using a general linear model. Group-level analyses were conducted using a fixed-effect model to quantify evoked responses across all subjects. Activated voxels in response to the heat stimulus were thresholded at $t > 1$ and registered to MTC anatomical images for display. The percentage BOLD signal changes of the selected region of interests (ROIs), identified from the heat activation map, were also calculated. A total of 26 heat stimulus runs were included in the statistical analysis.

2.3.3. Resting-state functional magnetic resonance imaging data analysis

Voxel-wise seed-based resting-state fMRI correlation analysis was performed using a customized rsFC toolbox in SPM 12 and MATLAB 2021b. This analysis calculated the Pearson correlation coefficient (r) between a chosen voxel (the seed) and all other voxels within the spinal cord. A correlation threshold of $r > 0.55$ ($P < 8.2 \times 10^{-5}$) was chosen to display significantly correlated voxels.[17,43,49]

The rsFC analysis between the GM horns was focused on the middle 3 slices representing the L3, L3/L4, and L4 spinal cord segments. A ROI-based pairwise correlation analysis was conducted between rsfMRI signal time series extracted from 4 manually defined GM horns (left and right dorsal horn: LD and RD, left and right ventral horn: LV and RV) and 1 white matter (WM) ROI, and correlation coefficients (r value) were derived. Detailed methods were described in our previous publications.[3,7] Within each slice, 8 pairwise correlations were computed: LD-LV, LD-RD, LD-RV, LV-RD, LV-RV, RD-RV, LD/RD-WM, LV/RV-WM. The statistical difference in rsFC between the ROI pairs was compared using the nonparametric Mann-Whitney–Wilcoxon (MWW) test. Bonferroni correction was applied to account for multiple comparisons.

The reproducibility of within-slice rsFC was also examined. A total of 40 resting-state fMRI runs from 9 rats were split into odd and even runs. Inter-ROI correlations computed within each slice (3 slices in total, L3-L4) were averaged. The resulting average correlations from the odd-numbered runs and even-numbered runs were paired for linear regression analysis. The r values and P values between the 20 paired runs were calculated to quantify the reproducibility of the resting-state inter-ROI correlation. The Bland–Altman method was used to evaluate the agreement of r values between odd and even runs by computing the upper and lower 95% limits of agreement.

3. Results

3.1. Functional magnetic resonance imaging image quality at the lumbar spinal cord

Figure 1 presents the representative structural MTC image of L3-L5 segments of a healthy rat spinal cord. The lumbar enlargement becomes evident starting from the second slice. The averaged tSNR of the middle 3 slices of rats improves from 29.4 ± 0.75 to 39.6 ± 1.6 after preprocessing. The GM and WM are distinguishable in axial, sagittal, and coronal views.

3.2. Functional magnetic resonance imaging activation pattern to noxious heat stimulation of left hind paw

Noxious heat-evoked fMRI activations were detected (**Fig. 2A**, thresholded at $t = 1$), with bilateral activation at the deep layers of both LD and RD at slice 2 (L3) and intermediate zones. On slice 4 (L4), fMRI activation was localized to the deep layer of LD on the same side of the hind paw being stimulated. No activation was observed on slice 3 (L3/L4). The percentage of BOLD signal changes extracted from ROI 1 in the LD and ROI 4 in the WM is plotted in **Figure 2B**. Numerical values are summarized in **Table 1**.

BOLD time courses exhibited standard hemodynamic response functions. The signal change in ROI 1 peaked approximately 15 seconds after the stimulus onset. The time course in ROI 2 peaked at 12.8 seconds, while ROI 3 peaked at 15 seconds. By contrast, the time course extracted from the WM (ROI 4) exhibited negligible signal fluctuations around the baseline.

3.3. Reproducible resting-state correlation pattern across animals

We examined voxel-wise resting-state correlation maps using seeds placed at the center of either dorsal or ventral GM horns of the L4 segment (slice 4) in 5 representative rats. Applying a display cutoff threshold of $r > 0.55$, we observed consistent and reproducible strong rsFC between LD-RD and LV-RV. In some rats, such as Rat 3, strong correlations were also detected between RD-RV or between RD and the intermediate zone (**Fig. 3**).

3.4. Functional connectivity between gray matter horns within and across spinal segments

Within slice 2 (L3), slice 3(L3/L4), or slice 4 (L4), the rsFC strengths between LV-RV ($r = 0.50, 0.53, 0.52$, respectively) were significantly ($P < 0.05$, MWW test) stronger than those of LD-RV ($r = 0.36, 0.36, 0.33$) and LV-RD ($r = 0.33, 0.33, 0.20$) (**Fig. 4**). For the L3 segment, LD-RD ($r = 0.46$) was more strongly correlated than LV-RD ($r = 0.33$) ($P < 0.05$). For the L4 segment, significantly stronger correlations ($P < 0.01$) between LD-RD ($r = 0.44$) than RD-LV ($r = 0.20$) or RD-RV ($r = 0.21$) were observed. However, at L3/L4, no GM horns showed significant correlation to LD-RD ($r = 0.46$). The mean rsFC strengths for RD-LV/RD-RV averaged over slices 2-3 ($r = 0.33$ and 0.41) are significantly higher than those at slice 4 ($r = 0.20$ and 0.21; $P < 0.05$). As controls, correlations between dorsal or ventral horns and the WM ROI were markedly weaker (the last 2 gray shaded columns in **Fig. 4**).

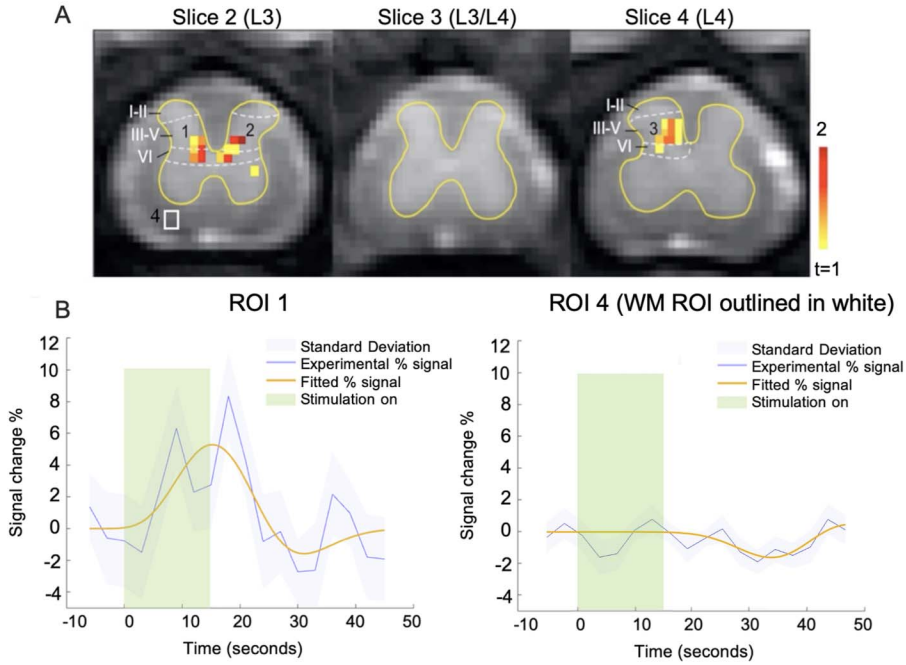

Figure 2. Group-level heat stimulus-evoked fMRI activation map and BOLD time courses. (A) BOLD activation map thresholded at $t > 1$ (with Benjamin–Hochberg false discovery rate correction). Data from 9 rats and 26 runs are included in the analysis. The activated regions are labeled as ROIs 1 to 3 on the group activation map. ROI 4, outlined by a white square, represents a white matter ROI. The gray–white matter boundary is outlined by yellow lines. White dashed lines indicate the approximate borders between the superficial (lamina I–II), deep (lamina III–IV), and intermediate layers (lamina VI). (B) The averaged percentage BOLD signal change time courses were extracted for the ROI 1 and white matter ROI 4 in slice 2. Heat stimulation was presented at 15 seconds on and 30 seconds off cycles.

We also quantified the correlation coefficients between corresponding GM horns across segments on neighboring slices along the L3-L4 segments, as schematically illustrated in **Figure 5A**. The averaged *r* values between GM horns on adjacent slices were around 0.001 (**Fig. 5B**), with no significant differences detected.

3.5. Reproducibility of functional connectivity between gray matter horns within slice

R values between the rsFC at odd and even runs collected from all 9 rats were compared, as depicted in **Figure 6** (left panels of each subplot). Significant correlations were observed between them for all 6 GM pairs. Among these, LD-RD ($r = 0.83$, $P < 0.0001$) and LV-RV ($r = 0.71$, $P = 0.0007$) exhibited the highest reproducibility at L3 to L4 spinal cord. In addition, no significant differences in reproducibility were observed for LD-LV ($r = 0.61$, $P = 0.0042$), LD-RV ($r = 0.60$, $P = 0.0053$), LV-RD ($r = 0.67$, $P = 0.0011$), and RD-RV ($r = 0.60$, $P = 0.0001$). Reproducible horn–horn rsFC were observed in all 6 ROI pairs, although their strengths varied. Bland–Altman plots (**Fig. 6**, right panel of each subplot) illustrate the agreement between odd and even runs. We found that LD-RD and LV-RV pairs exhibited comparatively smaller differences in *r* values between

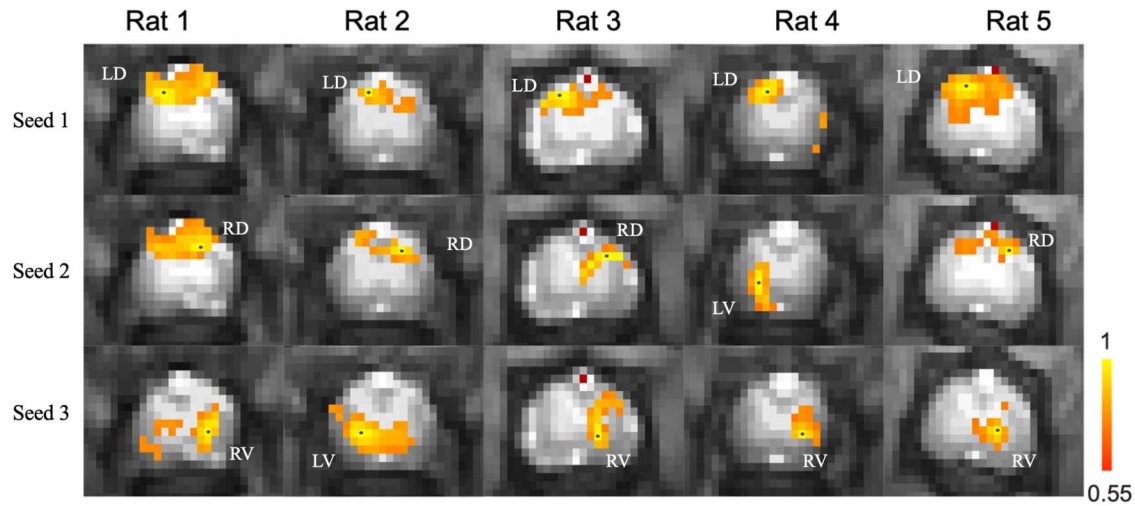

Figure 3. Examples of within-slice seed-based correlation maps at slice 4 (L4) across 5 representative animals with a cutoff threshold of $r > 0.55$. The seed voxel is marked with a black asterisk.

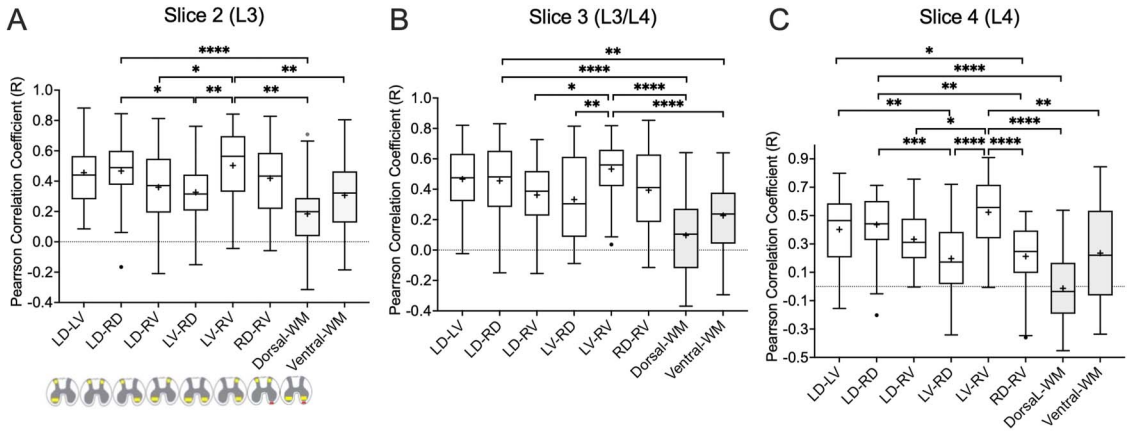

Figure 4. Box plots of correlation coefficient values between intraslice spinal horns on 3 slices (L3–L4). (A–C) The center lines represent the median of data; the whiskers represent the range within 1.5 times the difference between the third and first quartile of data. The mean is marked as "+." The dots represent the outliers. *$P < 0.05$, **$P < 0.01$, ***$P < 0.001$, ****$P < 0.0001$(Mann-Whitney–Wilcoxon test, Bonferroni corrected); data from 9 rats and 40 runs are included in the quantification. LD, left dorsal horn; LV, left ventral horn; RD, right dorsal horn; RV, right ventral horn; WM, white matter.

odd and even runs and range of limits than those of dorsal–ventral horn connections.

3.6. Functional connectivity alterations after heat stimulation

We also compared within-slice horn–horn rsFCs before and after approximately 30 minutes heat stimulation and observed no significant differences at slice 2 (L3) and slice 3 (L3/L4) (**Figs. 7A and B**). However, at slice 4 (L4), heat stimulation led to a significant decrease in the correlation between LD and RV, with *r* value dropping from 0.39 to 0.20 (**Fig. 7C**).

3.7. Resting-state functional connectivity between nociceptive heat processing regions

To determine whether dorsal horn regions involved in nociceptive heat processing exhibit stronger rsFC, we quantified the correlation strength between spinal cord regions that exhibited BOLD activation to heat stimulation. **Figure 8A** shows boxplots of the r values between the 3 heat-responsive ROIs (ROIs 1–3, shown in **Fig. 2**). Resting-state functional connectivity strength between ROI 1 and ROI 2 ($r = 0.68$) is significantly higher ($P < 0.0001$) than LD-RD in slice 2 ($r = 0.47$) (**Figs. 8A and B**). However, the correlation values between ROI 1-ROI 3 and ROI 2-ROI 3 were close to 0 (**Fig. 8A**) and were not significantly different from the intersegment correlation strengths between the RDs at slice 2 and slice 4 (**Fig. 8C**).

4. Discussion

4.1. Nociceptive heat processing networks within the lumbar spinal cord

At the lumbar L4 spinal cord, localized fMRI activation was observed in the ipsilateral dorsal horn (LD), where noxious heat of 47.5°C was applied to the hind paw. This observation of an ipsilateral fMRI response to the stimulus is consistent with previous reports in the rat lumbar cord, nonhuman primate (NHP) cervical cord, and human cervical spinal cord.[5,7,28,32,34,39,40,51] It further confirms that dorsal horns on the same side as the unilateral noxious heat stimulation serve as the main processing station for nociceptive inputs coming from the hindlimb.

In this study, the hind paw heat (47.5°C) stimulation-evoked fMRI activation was primarily detected in the deep layer of the L4 ipsilateral dorsal horn as well as in the bilateral deeper layer and intermediate zone of the L3 segment (**Fig. 2**). This overall activation pattern differs from what was reported in nonhuman primate cervical spinal cord and human spinal studies[7,11,35,40,51] in which noxious heat-evoked fMRI responses were located primarily in the superficial layers of the dorsal horn within the cervical spinal cord enlargement. One possible explanation is that the deep layer predominantly processes nociceptive heat information in the rat lumbar enlargement. It is known that both superficial and deeper layers are involved in processing nociceptive inputs,[16,19,47] and it is likely that the long-lasting (15

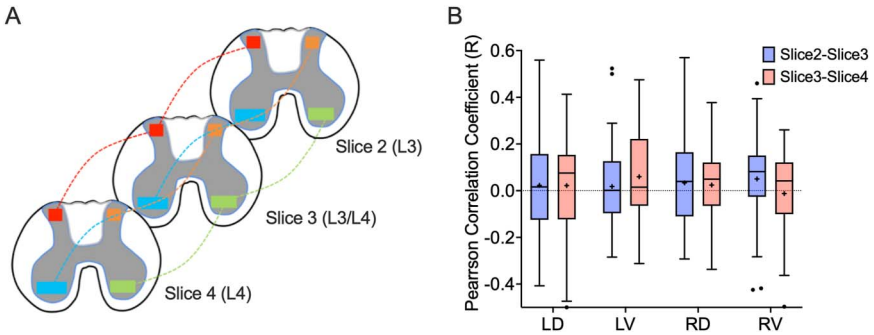

Figure 5. Group analysis of intersegmental functional connectivity between spinal cord gray matter horns on adjacent slices. (A) Schematic illustration of intersegment pairwise comparisons. (B) Box plots of *r* values between the horns of slice 2 and slice 3 and between the horns of slice 3 and slice 4.

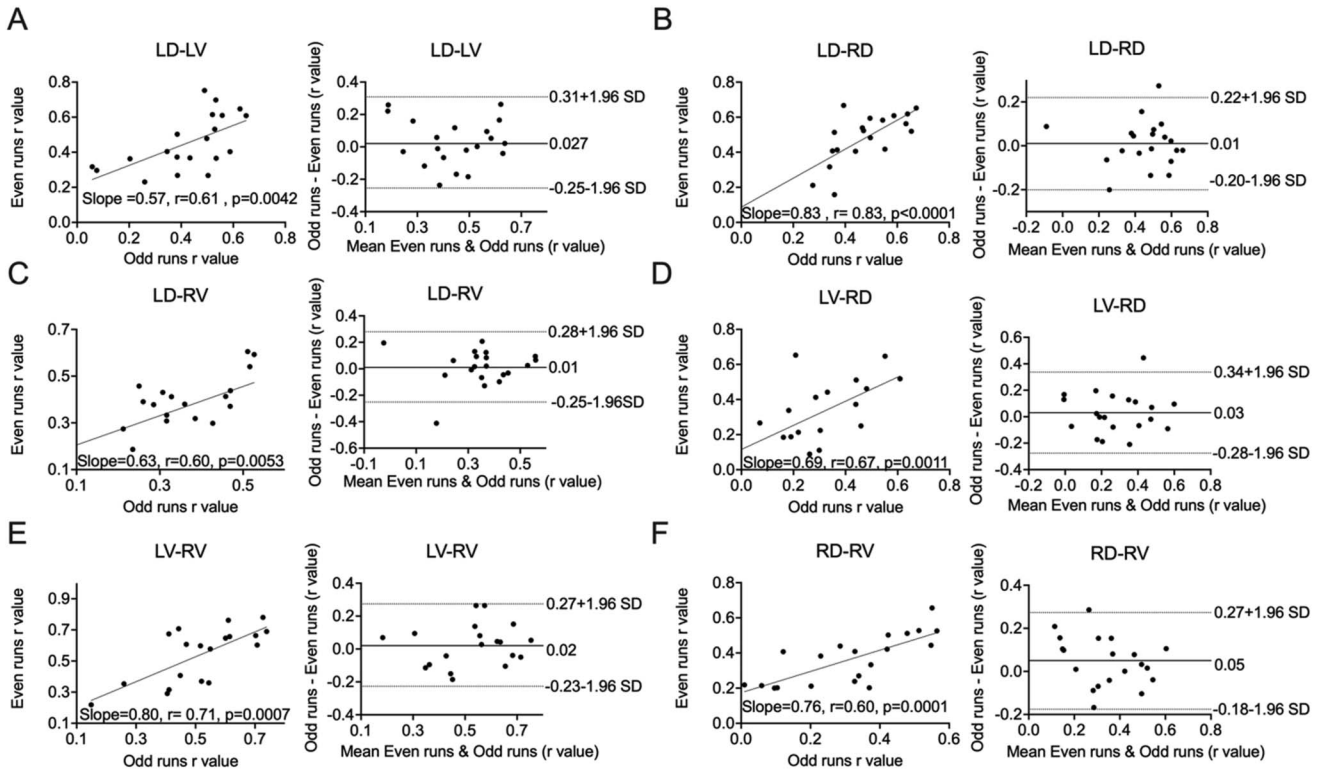

Figure 6. Reproducibility of averaged within-slice horn-to-horn correlation coefficients. Scatter plots of odd runs *r* values against even runs (left panel) and Bland–Altman plots of difference in *r* values between odd and even runs against mean *r* values of even and odd runs (right panel) for each horn pair: (A) LD-LV, (B) LD-RD, (C) LD-RV, (D) LV-RD, (E) LV-RV, (F) RV-RD. Each point represents the averaged *r* values of slice 2 to 4 from neighboring odd and even runs. In scatter plots, solid lines represent the line of best fit. In Bland–Altman plots, solid lines represent the mean difference between odd and even groups, and dotted lines show the 95% limits of agreement.

seconds) noxious heat stimulus activated afferents that predominantly terminate in the deep layer of the rat's lumbar dorsal horn.

In addition, Aα fibers, which primarily transmit proprioceptive information from the dorsal ganglion root to laminae V and VI as parts of the sensory-motion circuit, may also be activated by 47.5°C heat.[16,41] Projection neurons, which transfer nociceptive heat inputs from the lower body to the brain, are dispersed throughout laminae III–VI.[47] Therefore, the Aδ, Aα fibers, and projection neurons could all potentially contribute to the detected noxious heat stimuli-evoked BOLD activation in the deep layers.[10,16] Consistent with previous studies, we observed fMRI activation at L4 spinal cord during stimulation of the rat hind paw.[1,33]

Importantly, we observed heat-evoked activations in the deeper and intermediate layers of bilateral dorsal horns at the L3 level (slice 2), which is the rostral end of the lumbar enlargement. The existence of high-level integrative processing circuits for sensory information has been reported in the L2/L3 spinal cord segments.[2,24,29,32] The widespread bilateral activation detected at the L3 spinal cord could reflect its function and support the notion that the L3 segment likely serves as a rostral modulation center for the functions of the spinal segments of the lumbar enlargement that controls the hindlimb movements.

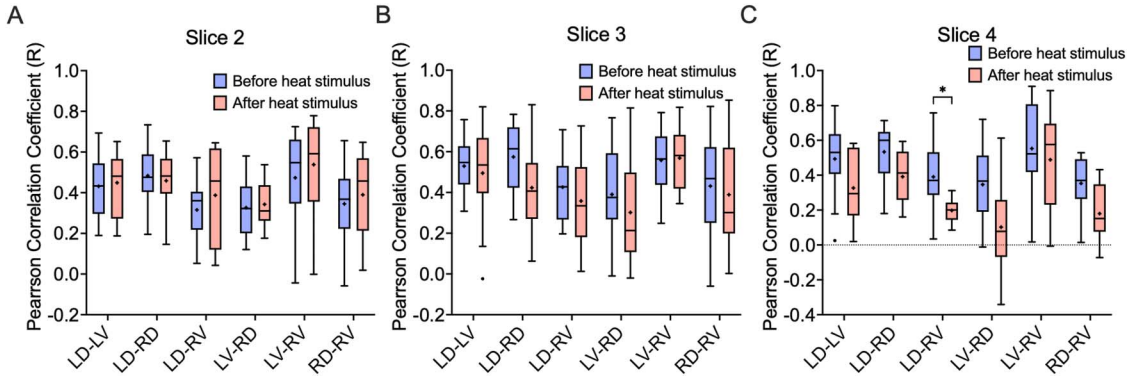

Figure 7. Comparison of the box plots of averaged r values between spinal cord gray matter horns before and after heat stimulation of the left hindlimb. The interhorn *r* values before and after heat stimulation in (A) slice 2, (B) slice 3, and (C) slice 4 . *$P < 0.05$ (Mann-Whitney–Wilcoxon test, Bonferroni-corrected).

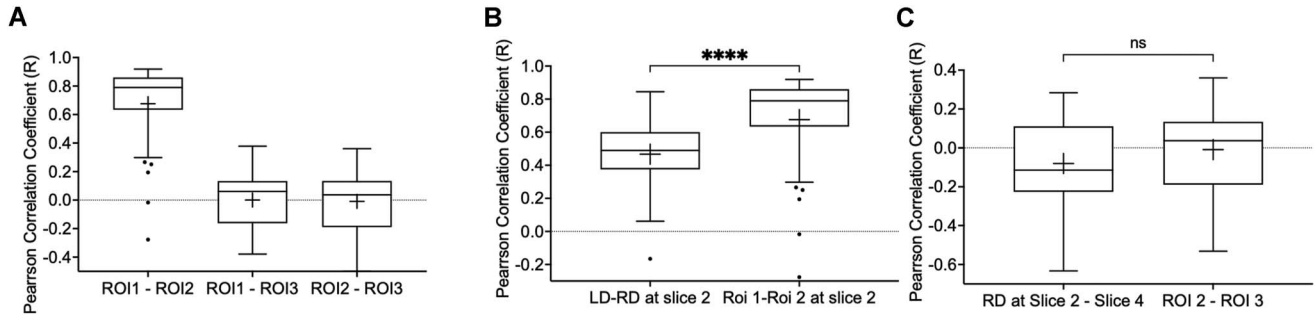

Figure 8. Comparisons of functional connectivity between functionally versus anatomically defined ROIs. Box plots of *r* values between (A) heat-responsive ROIs 1 to 3. (B) LD-RD and ROI1-ROI2 at slice 2. (C) ROI2-ROI3 and RDs at slice 2 and slice 4.

Future anatomical tracing and electrophysiological studies of these 2 functionally distinct spinal segments are needed to fully understand their roles in nociceptive processing and modulation.

4.2. Intrinsic functional connectivity networks of gray matter horns within lumbar spinal cord

Resting-state fMRI data analysis enables us to characterize the intrinsic functional connectivity pattern within the lumbar spinal cord. rsFC strengths between spinal GM horns seem comparable across spinal cord regions (cervical vs lumbar) and species. Studies on the human cervical spinal cord report that the within-slice rsFC between GM horns ranges from 0.18 to 0.44 at 1.5T[46] and 0.2 to 0.67 at 7T.[4] In the rat spinal cord, it ranges from 0.35 to 0.53 in the cervical region at 9.4T[49] and from 0.20 to 0.53 in the lumbar cord reported in this study. In the human lumbar spinal cord, it ranges from 0.22 to 0.64 at 3T.[46] In this study, we detected strong intrinsic rsFC between LD-RD and LV-RV in the rat lumbar spinal cord, consistent with previous findings in the rats' cervical spinal cord studies from our group.[49] Together, these stronger intrinsic connections between bilateral sensory or motor horns could be attributed to their engagement in coordinating bilateral limb behavior in rodents. By contrast, within the human cervical spinal cord, stronger connections are observed between dorsal sensory and ventral motor horns on the same side.[4,8,13,18,23,26,45] Compared with NHPs and humans, rodents use their hindlimbs differently. These differences in interhorn connectivity strength could reflect functional and behavioral differences between rodents and humans. The behavior of human limbs may engage more sensory and motor integration on the same side, while rodent limbs engage more bilateral integration for sensory and motor behaviors.

The intrinsic rsFC strength varies slightly across cervical segments, generally decreasing from C2 to C8.[13] However, the pattern of strong LD-RD and LV-RV connection remains unchanged. This feature was also observed in the lumbar spinal cord. In this study, we observed a decrease in rsFC between the RD-LV and RD-RV in L4 segment compared with more rostral segments (L3). Regarding intersegment connectivity between GMHs, we found no significant correlation, consistent with observations in human and rat cervical spines.[23,49] However, in nonhuman primates, strong intersegmental and interhorn connectivity has been observed.[35] We hypothesize that these interspecies connectivity pattern differences reflect their underlying functional organization that is closely related to behavior.[4,26]

Interestingly, in our study, we also observed a decrease in the *r* value between GM connections at the L4 segments after processing a heat stimulus. Disruptions and weakening in rsFC networks have been observed in the nonhuman primate cervical cord after injury.[7] The reason for the weakened connection between GM regions after processing heat nociceptive inputs warrant further investigation.

Table 1

Activated region's corresponding averaged percentage signal change based on stimulus paradigm.

Region of interests	ROI 1 (L3)	ROI 2 (L3)	ROI 3 (L4)	ROI 4 (WM)
% signal change	5.28 ± 2.63	4.15 ± 2.10	0.63 ± 0.86	0 ± 0.78

ROI, region of interest.

4.3. Reproducibility of resting-state functional connectivity in lumbar gray matter horns

We reported the highest reproducibility in rsFC between LD-RD and LV-RV connections in the rat lumbar spinal cord, while the reproducibility in rsFC between dorsal–ventral (LD-LV, RD-RV, LD-RV, and RD-LV) comparisons was much weaker. A similar pattern was also observed in the human cervical spinal cord at 7T.[46] As reported, the reproducibility of the within-slice rsFC between LV-RV and LD-RD connections is 0.71 to 0.83. The reproducibility of dorsal–ventral connections, where $r = 0.60$ to 0.67, is significantly weaker ($P < 0.05$). Our study reported a significantly high reproducibility in rsFC between all GM horns, with LV-RV connections being lower than that for LD-RD. This finding contrasts with results from Wu's cervical cord study,[49] although a similar imaging acquisition and preprocessing protocol was used. We do not attribute this difference to image quality, as tSNR and spatial SNR in cervical vs lumbar fMRI images did not differ significantly. Other factors, such as biological differences between the cervical and lumbar spinal cord, may contribute to this variation. For instance, motor neuron networks in the lumbar cord have been reported to exhibit longer cluster distances and higher network degree compared with those in the cervical region,[6] suggesting a more spatially distributed organization. This could result in differing degrees of signal synchronization across the ventral horns, potentially reducing the reproducibility of ventral–ventral rsFC in the lumbar cord.

4.4. Stronger resting-state functional connectivity between nociceptive processing regions

In ROI-based rsFC analysis, the selection of ROIs is critical for subsequent analysis and interpretation. Typically, there are 2 ways to identify seeds—using either anatomical or functional information. Performing rsFC analysis using functionally defined ROIs assumes that spinal cord regions involved in the same task likely exhibited stronger synchronized rsfMRI signal fluctuation.

As an example, our previous study of the monkey cervical cord demonstrated that functionally relevant regions exhibit stronger rsFC.[7] Supporting this notion, we found that the resting-state correlation strengths among the 3 nociceptive processing regions (ROIs 1–3) were higher than those among anatomically defined dorsal horns in the rat lumbar cord. Specifically, ROI 1 and ROI 2, located in the deep and intermediate layers of GM in the L3 segment, represent regions activated in response to heat stimulation. These 2 regions exhibited significantly higher rsFC within the L3 segment compared with LD-RD connections. This finding aligns with previous studies on human and NHP cortical regions, as well as the NHP cervical spinal cord.[7,9,25,31,44] It further substantiates that spinal regions involved in the same function, such as heat processing in our case, exhibit stronger intrinsic rsFC than anatomically defined spinal cord horns.

In addition, we found that the rsFC between ROI 1 and ROI 3, ROI 2 and ROI 3, as well as the intersegment GM horns, was relatively weak, with r values close to 0. The finding of low rsFC after we move 1 slice away is also observed in Wu's rat cervical study.[49] We hypothesize that this could be because 1 subsegment of the lumbar spinal cord represents 1 functional unit, as more than 1 slice covers the enlargement.

4.5. Limitations of the study

We acknowledge that this study is based on a relatively small sample size. Two main technical challenges associated with lumbar spinal cord fMRI may have influenced our findings. The first challenge is motion artifacts caused by chest movement,[15] which are more pronounced in spinal segments located near the lungs. Although motion correction was applied, these artifacts may still have reduced the tSNR in those segments, potentially compromising the estimation of rsFC and the detection of BOLD signal changes induced by heat stimuli. The second challenge involves partial volume effects when imaging the small cross-sectional area of the spinal cord, which can also lower the SNR. At an in-plane resolution of 0.25×0.25 mm^2, each dorsal horn is sampled by approximately 5 voxels. Despite these limitations, both rsFC and heat stimulus-evoked BOLD signal changes were robustly detected. We attribute this sensitivity to the high MRI field strength (9.4 T) and the use of a customized surface coil.

5. Conclusion

In this study, using BOLD fMRI at 9.4T, we identified 2 nociceptive processing regions: ipsilateral dorsal horn of L3 and L4 in the deep layers and intermediate zones in L3. These heat-responsive regions showed stronger rsFC than the anatomically defined spinal horns. Consistent with the findings in the rat and primate cervical spinal cord, strong resting-state functional connections were observed between bilateral dorsal and ventral horns and no significant intersegment resting connectivity was observed.

Disclosures

The authors declare that they have no competing financial interests or personal relationships that appeared to influence the work reported in this article.

Acknowledgments

Author contributions: Conceptualization: X.Z., L.M.C. Software: M.A. Data Acquisition: F.W., C.M., X.Z., P.F.Y., X.Y., M.L. Data Analysis: X.Z. Manuscript Writing: X.Z. Manuscript Revision: X.Z., L.M.C., X.Y., F.W., C.M., J.C.G. Funding acquisition and project supervision: J.C.G., L.M.C.

Projects are supported by NIH Grant S10 OD025085 and CDMRP W81XWH2010648 SC190134.

Data and code availability: Data are not currently publicly available as this paper represents only a partial data set. The complete data set will be made available upon publication.

Article history:
Received 23 December 2024
Received in revised form 27 July 2025
Accepted 4 August 2025
Available online 11 February 2026

References

[1] Abbadie C, Honoré P, Besson JM. Intense cold noxious stimulation of the rat hindpaw induces c-*fos* expression in lumbar spinal cord neurons. Neuroscience 1994;59:457–68.
[2] Antri M, Mellen N, Cazalets J-R. Functional organization of locomotor interneurons in the ventral lumbar spinal cord of the newborn rat. PLoS One 2011;6:e20529.
[3] Barry RL, Rogers BP, Conrad BN, Smith SA, Gore JC. Reproducibility of resting state spinal cord networks in healthy volunteers at 7 Tesla. Neuroimage 2016;133:31–40.
[4] Barry RL, Smith SA, Dula AN, Gore JC. Resting state functional connectivity in the human spinal cord. eLife 2014;3:e02812.
[5] Bosma RL, Ameli Mojarad E, Leung L, Pukall C, Staud R, Stroman PW. Neural correlates of temporal summation of second pain in the human brainstem and spinal cord. Hum Brain Mapp 2015;36:5038–50.
[6] Bukreeva I, Campi G, Fratini M, Spanò R, Bucci D, Battaglia G, Giove F, Bravin A, Uccelli A, Venturi C, Mastrogiacomo M, Cedola A. Quantitative 3D investigation of neuronal network in mouse spinal cord model. Sci Rep 2017;7:41054.
[7] Chen LM, Mishra A, Yang P-F, Wang F, Gore JC. Injury alters intrinsic functional connectivity within the primate spinal cord. Proc Natl Acad Sci 2015;112:5991–6.
[8] Combes A, Narisetti L, Sengupta A, Rogers BP, Sweeney G, Prock L, Houston D, McKnight CD, Gore JC, Smith SA, O'Grady KP. Detection of resting-state functional connectivity in the lumbar spinal cord with 3T MRI. Sci Rep 2023;13:18189.
[9] Deogaonkar M, Sharma M, Oluigbo C, Nielson DM, Yang X, Vera-Portocarrero L, Molnar GF, Abduljalil A, Sederberg PB, Knopp M, Rezai AR. Spinal cord stimulation (SCS) and functional magnetic resonance imaging (fMRI): modulation of cortical connectivity with therapeutic SCS. Neuromodulation 2016;19:142–53.
[10] Duan B, Cheng L, Bourane S, Britz O, Padilla C, Garcia-Campmany L, Krashes M, Knowlton W, Velasquez T, Ren X, Ross SE, Lowell BB, Wang Y, Goulding M, Ma Q. Identification of spinal circuits transmitting and gating mechanical pain. Cell 2014;159:1417–32.
[11] Duan W, Huang Q, Chen Z, Raja SN, Yang F, Guan Y. Comparisons of motor and sensory abnormalities after lumbar and thoracic contusion spinal cord injury in male rats. Neurosci Lett 2019;708:134358.
[12] Eippert F, Finsterbusch J, Bingel U, Büchel C. Direct evidence for spinal cord involvement in placebo analgesia. Science 2009;326:404.
[13] Eippert F, Kong Y, Winkler AM, Andersson JL, Finsterbusch J, Büchel C, Brooks JCW, Tracey I. Investigating resting-state functional connectivity in the cervical spinal cord at 3 T. Neuroimage 2017;147:589–601.
[14] Endo T, Spenger C, Westman E, Tominaga T, Olson L. Reorganization of sensory processing below the level of spinal cord injury as revealed by fMRI. Exp Neurol 2008;209:155–60.
[15] Fratini M, Moraschi M, Maraviglia B, Giove F. On the impact of physiological noise in spinal cord functional MRI. J Magn Reson Imaging 2014;40:770–7.
[16] Furue H, Narikawa K, Kumamoto E, Yoshimura M. Responsiveness of rat substantia gelatinosa neurones to mechanical but not thermal stimuli revealed by in vivo patch-clamp recording. J Physiol 1999;521:529–35.
[17] Garrison KA, Scheinost D, Finn ES, Shen X, Constable RT. The (in)stability of functional brain network measures across thresholds. Neuroimage 2015;118:651–61.
[18] Harita S, Ioachim G, Powers J, Stroman PW. Investigation of resting-state BOLD networks in the human brainstem and spinal cord. Neuroscience 2019;404:71–81.
[19] Hillman P, Wall PD. Inhibitory and excitatory factors influencing the receptive fields of lamina 5 spinal cord cells. Exp Brain Res 1969;9:284–306.

[20] Jongen JLM, Holstege JC. Propagation of spinal nociceptive activity in the spatial and temporal domains. Neuroscientist 2012;18:8–14.
[21] Khan HS, Stroman PW. Inter-individual differences in pain processing investigated by functional magnetic resonance imaging of the brainstem and spinal cord. Neuroscience 2015;307:231–41.
[22] Koch SC, Acton D, Goulding M. Spinal circuits for touch, pain and itch. Annu Rev Physiol 2018;80:189–217.
[23] Kong Y, Eippert F, Beckmann CF, Andersson J, Finsterbusch J, Büchel C, Tracey I, Brooks JCW. Intrinsically organized resting state networks in the human spinal cord. Proc Natl Acad Sci U S A 2014;111:18067–72.
[24] Konya D, Liao W-L, Choi H, Yu D, Woodard MC, Newton KM, King AM, Pamir NM, Black PM, Frontera WR, Sabharwal S, Teng YD. Functional recovery in T13-L1 hemisected rats resulting from peripheral nerve rerouting: role of central neuroplasticity. Regen Med 2008;3:309–27.
[25] Kowalski JL, Morse LR, Troy K, Nguyen N, Battaglino RA, Falci SP, Linnman C. Resting state functional connectivity differentiation of neuropathic and nociceptive pain in individuals with chronic spinal cord injury. Neuroimage 2023;38:103414.
[26] Liu X, Zhou F, Li X, Qian W, Cui J, Zhou IY, Luk KDK, Wu EX, Hu Y. Organization of the intrinsic functional network in the cervical spinal cord: a resting state functional MRI study. Neuroscience 2016;336:30–8.
[27] Lu M, Drake G, Wang F, Mu C, Chen LM, Gore JC, Yan X. Design and construction of an interchangeable RF coil system for rodent spinal cord MR imaging at 9.4 T. Magn Reson Imaging 2021;84:124–31.
[28] Malisza KL, Stroman PW, Turner A, Gregorash L, Foniok T, Wright A. Functional MRI of the rat lumbar spinal cord involving painful stimulation and the effect of peripheral joint mobilization. J Magn Reson Imaging 2003;18:152–9.
[29] Matsushita M. Projections from the lowest thoracic and upper lumbar segments to the cerebellar cortex in the rat: an anterograde tracing study. Neurosci Res 2021;170:166–80.
[30] Meuwissen KPV, van der Toorn A, Gu JW, Zhang TC, Dijkhuizen RM, Joosten EAJ. Active recharge burst and tonic spinal cord stimulation engage different supraspinal mechanisms: a functional magnetic resonance imaging study in peripherally injured chronic neuropathic rats. Pain Pract 2020;20:510–21.
[31] Mishra A, Majumdar S, Wang F, Wilson GH, Gore JC, Chen LM. Functional connectivity with cortical depth assessed by resting state fMRI of subregions of S1 in squirrel monkeys. Hum Brain Mapp 2019;40:329–39.
[32] Ohtori S, Takahashi K, Yamagata M, Sameda H, Moriya H, Chiba T, Takahashi Y. Neurones in the dorsal root ganglia of T13, L1 and L2 innervate the dorsal portion of lower lumbar discs in rats. A study using dil, an anterograde neurotracer. J Bone Joint Surg Br 2001;83-B:1191–4.
[33] Ota H, Takebe H, Mizumura K, Taguchi T. Responses of cutaneous C-fiber afferents and spinal microglia after hindlimb cast immobilization in rats. J Physiol Sci 2021;71:19.
[34] Rempe T, Wolff S, Riedel C, Baron R, Stroman PW, Jansen O, Gierthmühlen J. Spinal and supraspinal processing of thermal stimuli: an fMRI study. J Magn Reson Imaging 2015;41:1046–55.
[35] Sengupta A, Mishra A, Wang F, Li M, Yang P-F, Chen LM, Gore JC. Functional networks in non-human primate spinal cord and the effects of injury. Neuroimage 2021;240:118391.
[36] Smith SM, Jenkinson M, Woolrich MW, Beckmann CF, Behrens TEJ, Johansen-Berg H, Bannister PR, De Luca M, Drobnjak I, Flitney DE, Niazy RK, Saunders J, Vickers J, Zhang Y, De Stefano N, Brady JM, Matthews PM. Advances in functional and structural MR image analysis and implementation as FSL. Neuroimage 2004;23(suppl 1):S208–19.
[37] Sprenger C, Eippert F, Finsterbusch J, Bingel U, Rose M, Büchel C. Attention modulates spinal cord responses to pain. Curr Biol 2012;22:1019–22.
[38] Sprenger C, Finsterbusch J, Büchel C. Spinal cord-midbrain functional connectivity is related to perceived pain intensity: a combined Spino-Cortical fMRI study. J Neurosci 2015;35:4248–57.
[39] Stroman PW, Bosma RL, Tsyben A. Somatotopic arrangement of thermal sensory regions in the healthy human spinal cord determined by means of spinal cord functional MRI. Magn Reson Med 2012;68:923–31.
[40] Summers PE, Ferraro D, Duzzi D, Lui F, Iannetti GD, Porro CA. A quantitative comparison of BOLD fMRI responses to noxious and innocuous stimuli in the human spinal cord. Neuroimage 2010;50:1408–15.
[41] Todd AJ. Neuronal circuitry for pain processing in the dorsal horn. Nat Rev Neurosci 2010;11:823–36.
[42] Toossi A, Bergin B, Marefatallah M, Parhizi B, Tyreman N, Everaert DG, Rezaei S, Seres P, Gatenby JC, Perlmutter SI, Mushahwar VK. Comparative neuroanatomy of the lumbosacral spinal cord of the rat, cat, pig, monkey, and human. Sci Rep 2021;11:1955.
[43] van den Heuvel MP, Mandl RC, Kahn RS, Hulshoff Pol HE. Functionally linked resting-state networks reflect the underlying structural connectivity architecture of the human brain. Hum Brain Mapp 2009;30:3127–41.
[44] Wang Z, Chen LM, Négyessy L, Friedman RM, Mishra A, Gore JC, Roe AW. The relationship of anatomical and functional connectivity to resting-state connectivity in primate somatosensory cortex. Neuron 2013;78:1116–26.
[45] Weber KA, Sentis AI, Bernadel-Huey ON, Chen Y, Wang X, Parrish TB, Mackey S. Thermal stimulation alters cervical spinal cord functional connectivity in humans. Neuroscience 2018;369:40–50.
[46] Wei P, Li J, Gao F, Ye D, Zhong Q, Liu S. Resting state networks in human cervical spinal cord observed with fMRI. Eur J Appl Physiol 2010;108:265–71.
[47] Willis WD, Coggeshall RE. Sensory mechanisms of the spinal cord: Volume 1 primary afferent neurons and the spinal dorsal horn. Boston, MA: Springer US, 2004.
[48] Wu T-L, Byun NE, Wang F, Mishra A, Janve VA, Chen LM, Gore JC. Longitudinal assessment of recovery after spinal cord injury with behavioral measures and diffusion, quantitative magnetization transfer and functional magnetic resonance imaging. NMR Biomed 2020;33:e4216.
[49] Wu T-L, Wang F, Mishra A, Wilson GH III, Byun N, Chen LM, Gore JC. Resting-state functional connectivity in the rat cervical spinal cord at 9.4 T. Magn Reson Med 2018;79:2773–83.
[50] Yam MF, Loh YC, Tan CS, Khadijah Adam S, Abdul Manan N, Basir R. General pathways of pain sensation and the major neurotransmitters involved in pain regulation. Int J Mol Sci 2018;19:2164.
[51] Yang P-F, Wang F, Chen LM. Differential fMRI activation patterns to noxious heat and tactile stimuli in the primate spinal cord. J Neurosci 2015;35:10493–502.